DE TOC

Proceedings of IMECE'03
2003 ASME International Mechanical Engineering Congress
Washington, D.C., November 15–21, 2003

IMECE2003-43130

DECOMPOSITION-BASED ASSEMBLY SYNTHESIS OF A 3D BODY-IN-WHITE MODEL FOR STRUCTURAL STIFFNESS

Naesung Lyu and **Kazuhiro Saitou***
Department of Mechanical Engineering
University of Michigan
Ann Arbor, MI 48109-2125, USA
E-mail:{nlyu,kazu}@umich.edu

ABSTRACT
This paper presents an extension of our previous work on decomposition-based assembly synthesis for structural stiffness [1], where the 3D finite element model of a vehicle body-in-white (BIW) is optimally decomposed into a set of components considering the stiffness of the assembled structure under given loading conditions, as well as the manufacturability and assembleability of components. Two case studies, each focusing on the decomposition of a different portion of a BIW, are discussed. In the first case study, the side frame is decomposed for the minimum distortion of front door frame geometry under global bending. In the second case study, the side/floor frame and floor panels are decomposed for the minimum floor deflections under global bending. In each case study, multi-objective genetic algorithm [2,3] with graph-based crossover [4,5], combined with FEM analyses, is used to obtain Pareto optimal solutions. Representative designs are selected from the Pareto front and trade-offs among stiffness, manufacturability, and assembleability are discussed.

INTRODUCTION
Complex structural products such as automotive bodies are made of hundreds of components joined together. While a monolithic design is ideal from a structural viewpoint, it is virtually impossible to economically manufacture complex structures as one piece, requiring them to be assemblies of smaller sized components with simpler geometry. Therefore, during the conceptual design stage designers need to decide a set of components by decomposing the overall product geometry of the whole structure. In industry, a handful of basic decomposition schemes considering geometry, functionality, and manufacturing issues are used. However, these decomposition schemes are usually non-systematic and depend mainly on the designers' experience, which may cause the following problems during design and the production phases:

- *Problems of the insufficient assembled structure stiffness*: Components and joining methods specified by designers may not meet the desired stiffness of the assembled structure.
- *Problems of manufacturability and assembleability*: Components decided by designers can not be produced or assembled in an economical way.

Since these problems are directly related to the component and joint configurations and therefore usually found in the production phase, solving them requires costly and time-consuming iteration from an early design stage. Hence introducing more systematic method of finding components set considering overall structural characteristics, manufacturability and assembleability will have a significant impact on industry.

Assembly synthesis [6] refers to such a systematic method where entire product geometry is decomposed to components and joints. Since joints are often structurally inferior to components, it is important the decomposition and joint allocation are done in an optimal fashion, such that the reduction in structural performances (*eg*., stiffness) is maximized while achieving economical manufacture and assembly.

As an extension of our previous work on decomposition-based assembly synthesis for structural stiffness [1], the present method optimally decomposes the 3D finite element model of a vehicle body-in-white (BIW) into a set of components considering the stiffness of the assembled structure under given loading conditions, as well as the manufacturability and assembleability of components. The stiffness of the assembled structure is evaluated by FEM analyses, where joints are

* corresponding author

modeled as linear torsional springs. Manufacturability of a component is evaluated as a estimated manufacturing cost based on the size and geometric complexity of components. Assuming assembly efforts are proportional to the total number of weld spots, assembleability is simply accounted for as the total rate of torsional springs. In order to allow close examination of the trade-off among stiffness, manufacturability, and assembleability, the optimization problem is solved by a multi-objective genetic algorithm, which can efficiently generate a well-spread Pareto front over multiple objectives. A graph-based crossover scheme is adopted for the improved convergence of the algorithm.

RELATED WORK

Design for Assembly/Manufacturing

Design for assembly (DFA) and design for manufacturing (DFM) refers to design methodologies to improve product and process during the design phase of a product, thereby ensuring the ease of assembly and manufacturing. Boothroyd and Dewhurst [7] are widely regarded as major contributors in the establishment of DFA/DFM theories. In their work [8], assembly costs are first reduced by the reduction of part count, followed by the local design changes of the remaining parts to enhance their assembleability and manufacturability. One of the main functions of DFA/DFM is manufacturability analysis of the product design, *eg.*, by evaluating the capability of production within the specified requirements such as low production costs and short production time. In general, to manufacturability analysis requires a product to be decomposed into features containing a manufacturing meaning, such as, surfaces, dimensions, tolerances and their correlations [9].

While existing DFA/DFM methods share the idea of simultaneous engineering with the present approach, they analyze or improve existing designs from the viewpoint of assembly and manufacturing by modifying geometry of given (*i.e.*, already decomposed) components. On the other hand, the decomposed-based assembly synthesis method presented in this paper starts with no prescribed components and generates optimized components set considering assembleability, manufacturability and structural characteristic of the assembled structure.

Automotive Body Structure Modeling

In automotive body design, high stiffness is one of the most important design factors, since it is directly related the improved ride and NVH (Noise, Vibration, and Harshness) qualities and crashworthiness [10]. Therefore evaluating the structural characteristics of a vehicle, including stiffness, became a crucial factor in designing a vehicle.

Before mathematical modeling techniques were not available, structural analysis was usually carried out only for the stresses in specific hardware items, such as door hinges, drive train and suspension components. Overall structural behavior could not be predicted until a vehicle prototype was built and tested. Therefore, any changes recommended from the test results were bound to be costly to implement [11].

Prior to the use of Finite Element Methods(FEM) in the automotive body analysis in the middle of 1960s, preliminary structural analysis was performed by Simple Structural Surface method (SSS method) [12,13], where the actual vehicle geometry was replaced with an equivalent boxlike structure composed of shear panels and reinforcing beams. With SSS methods, designers can identify the type of loading condition that is applied to each of the main structural members of a vehicle and also the nominal magnitudes of the loads to be determined based on the static conditions with load path in the structure. However, this method can be used only to the simplified conceptual design and it can not be used to solve for loads on redundant structures with more than one load path [13].

The availability of high-powered computers, user-oriented FEM codes and economical solution methods enabled full-scale finite element vehicle models in the early 70's. To predict the stiffness of a body structure with finite element model more accurately, Chang [14] modeled joints as torsional springs, and demonstrated that the model can accurately predict the global deformation of automotive body substructures. Garro and Vullo [15] analyzed the dynamic behavior of typical body joints under two typical actual loading conditions. They addressed that the plates along spot welds tend to detach from each other when joint deformations occur. Lee and Nikolaidis [16] proposed a 2-D joint model to consider joint flexibility, the offset of rotation centers and coupling effects between the movements of joint branches. Recently, correlation between torsional spring properties of joints and the length of structural member was studied to assess the accuracy of joint model [17]. Long [18] studied the method of correlating the performance targets for a design of individual joint in the automotive to design variables that specify the geometry of the joint design. Kim, et al. [19] employed an 8-DOF beam theory for modeling joints to consider the warping and distortion in vibration analysis.

These works, however, focus on the accurate prediction of the structural behavior of a given (*i.e.*, already "decomposed") assembly and individual joint design and do not concern the selection of optimal joint locations and properties, which is addressed in the present method.

Multi-objective Optimization Algorithm

Engineering problems generally involves multiple objectives. Among the techniques to solve multi-objective optimization problems, evolutionary algorithms that simulate natural evolution process have shown to be effective in many engineering problems [20]. The major advantages of evolutionary algorithms in solving multiobjective optimization problems are 1) they can obtain Pareto optimal solutions in a single run, and 2) they do not require derivatives of objective functions.

Many evolutionary multiobjective optimization algorithms (MOGA [21], NSGA [22], NSGA-II [23], and NPGA [24]) were developed based on the two ideas suggested by Goldberg [25]: Pareto dominance and niching. Pareto dominance is used to exploit the search space in the direction of the Pareto front. Niching technique explores the search space along the front to keep diversity. Another important operator that has been shown to improve the performance of multiobjective algorithm is elitism, which maintains the knowledge of the previous generations by conserving the individuals with best fitness in the population or in an auxiliary population (SPEA [26] and PAES [27]).

Considering a proven efficiency and simplicity of NSGA-II, the present work utilizes an implementation based on NSGA-II with Pareto ranking selection.

DECOMPOSITION-BASED ASSEMBLY SYNTHESIS FOR STRUCTURAL STIFFNESS

Overview

The decomposition-based assembly synthesis method simultaneously identifies the optimal components set and joint attributes considering the stiffness of the assembled structure. It consists of the following two major steps:

1. A 3D finite element model is transformed to a *structural topology graph* representing the liaisons between *basic members*, the smallest decomposable components of the given structure, specified by the designer.
2. The product topology graph is automatically decomposed, through an optimization process, to a set of subgraphs representing components connected together by edges representing joints.

Detailed procedure covered throughout this section uses a simple structural model composed of a plate with reinforcing beam frame shown in Figure 1. This type of structure is widely used in automotive and airspace industries.

Step 1: Construction of structural topology graph

An entire structure is divided into substructures each of which can be manufactured by a single process (Figure 2 (b) and (c)). This prevents the synthesis of the components that cannot be manufactured with a single process. Then, basic members are defined in each substructure (Figure 2 (d) and (e)) by the designer. In this example, 4 basic members (B0~B3) are defined in the beam substructure and 6 basic members (P0~P5) are defined in the plate substructure. Since components are represented as a group of basic members, the definition of basic member determines the diversity and resolution of the resulting components.

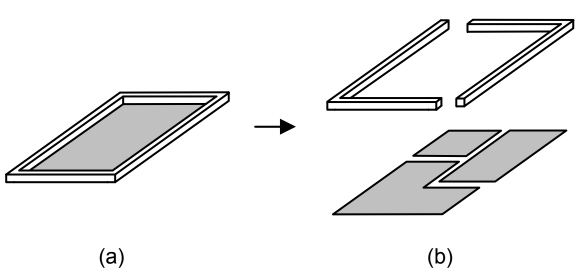

Figure 1. (a) simple structure with a plate reinforced by a beam, and (b) decomposition with 2 beam and 3 plate components.

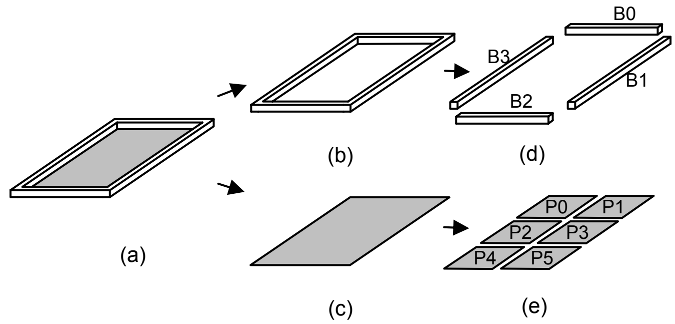

Figure 2. (a) Overall structure, (b) beam substructure and (c) plate substructure separated from (a), (d) 4 basic members (B0~B3) defined in (b), and (e) 6 basic members (P0~P5) defined in (c).

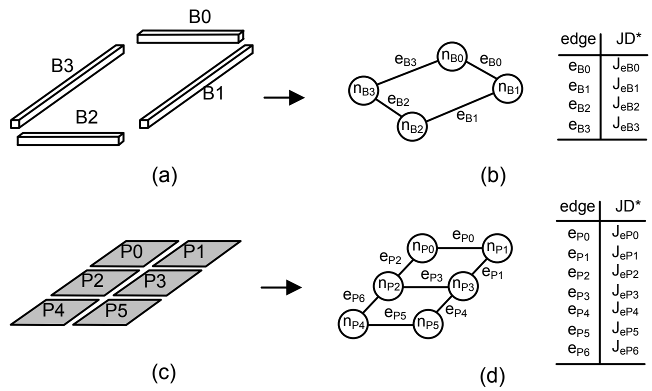

Figure 3. Constructing structural topology graph for eachsub structure. (a) basic members of beam substructure, (b) structural topology graph G_B of (a), (c) basic members of plate substructure, and (d) topology graph G_P of (c). In (b) and (d), JD* represents the joint design at each potential joint position defined for each edge.

Then, structural topology graph $G = (V, E)$ is constructed such that:

1. A basic member m_i is represented as a node n_i in set V.
2. The connections (liaisons) between two basic members m_i and m_j are represented as edge $e = \{n_i, n_j\}$ in set E.

As illustrated in Figure 3, structural topology graph G_B (Figure 3 (b)) of the beam substructure with 4 nodes (n_{B0}~n_{B3}) and 4 edges (e_{B0}~e_{B3}) is constructed based on the basic members of Figure 3 (a). Similarly, structural topology graph G_P (Figure 3 (d)) of the plate substructure with 6 nodes (n_{P0}~n_{P5}) and 7 (e_{P0}~e_{P6}) edge is constructed from the basic members in Figure 3 (c). Joints can occur at each connection between basic members. Hence, joint designs (JD), attributes of joints, are assigned to every edge in G_B and G_P (tables in Figure 3 (b) and (d)). In addition, the entire structural topology graph G_E is defined to represent the joints between substructures. In Figure 4, joint designs between the beam and plate components (Figure 4 (c)) are assigned to 10 edges between the beam and plate basic members (e_{BP0}~e_{BP9}) shown as thick edges in Figure 4 (b).

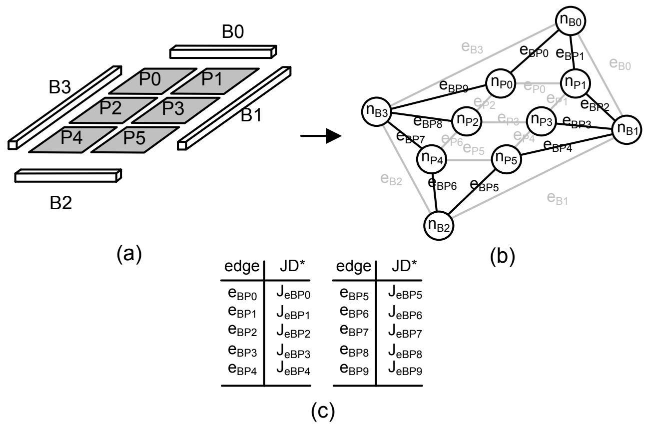

edge	JD*	edge	JD*
e_{BP0}	J_{eBP0}	e_{BP5}	J_{eBP5}
e_{BP1}	J_{eBP1}	e_{BP6}	J_{eBP6}
e_{BP2}	J_{eBP2}	e_{BP7}	J_{eBP7}
e_{BP3}	J_{eBP3}	e_{BP8}	J_{eBP8}
e_{BP4}	J_{eBP4}	e_{BP9}	J_{eBP9}

(c)

Figure 4. (a) beam and plate basic members, (b) entire structural topology graph G_E., and (c) joint designs between beam and plate basic members (thick edges in (b)).

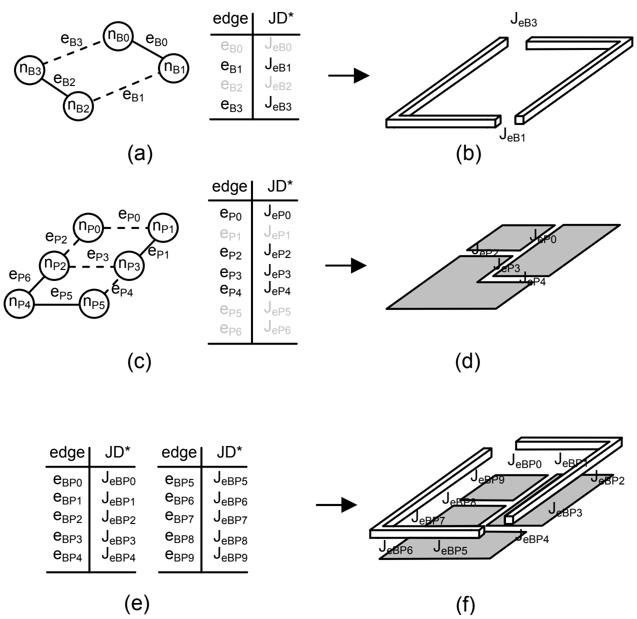

edge	JD*
e_{B0}	J_{eB0}
e_{B1}	J_{eB1}
e_{B2}	J_{eB2}
e_{B3}	J_{eB3}

edge	JD*
e_{P0}	J_{eP0}
e_{P1}	J_{eP1}
e_{P2}	J_{eP2}
e_{P3}	J_{eP3}
e_{P4}	J_{eP4}
e_{P5}	J_{eP5}
e_{P6}	J_{eP6}

edge	JD*	edge	JD*
e_{BP0}	J_{eBP0}	e_{BP5}	J_{eBP5}
e_{BP1}	J_{eBP1}	e_{BP6}	J_{eBP6}
e_{BP2}	J_{eBP2}	e_{BP7}	J_{eBP7}
e_{BP3}	J_{eBP3}	e_{BP8}	J_{eBP8}
e_{BP4}	J_{eBP4}	e_{BP9}	J_{eBP9}

Figure 5. Sample decomposition of structural topology graph of (a) beam substructure and (b) corresponding components set with joint designs, of (c) plate substructure and (d) corresponding components set with joint designs, (e) assignment of joint properties between beam and plate components, and (f) resulting component set.

Step 2: Decomposition of structural topology graph

Components set and joint designs between the components can be decided by choosing which edges will be removed in the structural topology graphs and by assigning appropriate joint designs at the location of removed edges. The joint designs are simply assigned to all joints between substructures (edges of entire structural topology graph G_E), since they must be always present.

In Figure 5 (a), edge e_{B1} and e_{B3} are chosen to be removed (shown in dotted lines) and the original G_B is decomposed into two subgraphs corresponding to the two beam components in Figure 5 (b). Note that only joint design J_{eB1} and J_{eB3} are realized in Figure 5 (b) because only edge e_{B1} and e_{B3} are removed and therefore joints are needed to connect components. The other joint designs (J_{eB0} and J_{eB1}) colored in gray in the table indicates that they are not realized. Similarly, by removing 4 edges (e_{P0}, e_{P2}, e_{P3} and e_{P4}) G_P is decomposed into 3 subgraphs corresponding to the three plate components in Figure 5 (d) with 4 joint designs (J_{eP0}, J_{eP2}, J_{eP3} and J_{eP4}) realized.

The quality of the component set and JD's are evaluated according to the following three objectives within an optimization loop:

1. **Stiffness of the assembled structure under given loading conditions:** it is evaluated as a displacement at a specific location of the assembled structure, calculated by FE analyses. To automatically generate FE models with joints during optimization, the default FE model that contains models for basic members (for example, Figure 3 (a) and (c)) is built. Then, by checking the modified structural topology graphs, basic members are connected using rigid FE elements (if the corresponding edge is present) or joint FE models (if the corresponding edge is removed) of the specified joint designs. In the following case studies, every joining is assumed to be done with spot welds, which are modeled as torsional springs in FE analysis.
2. **Manufacturability of components:** it is evaluated considering the total cost of producing components in the structure represented by decomposed product topology graphs G_B and G_P. It is assumed the components are made from sheet metal working, whose cost is estimated as the cost of stamping/blanking dies. In practice, die costs is usually represented as a function of die usable area Au. For each component, Au is approximated as the area of its convex hull. A larger component results in a higher value of Au, requiring larger die set with higher cost.
3. **Assembleability of components:** it is calculated considering the cost of assembly procedure. Since the cost of spot welding is proportional to the number of weld spots in the structure, and the number of weld spots in a joint is approximately proportional to the torsional stiffness of the joint, the welding cost is estimated by the sum of the rates of torsional springs [Nm/rad] in the FE model of the assembled structure.

Mathematical Formulation

Definition of design variables

A set of components and joint designs between the components can be defined by selecting edges to be removed in the two topology graphs (G_B and G_P) and by assigning joint designs at the location of removed edges. There are five design variables:

- $\boldsymbol{x}_B$: decomposition vector for G_B
- $\boldsymbol{x}_P$: decomposition vector for G_P
- $\boldsymbol{y}_B$: joint design vector for joints between beam components
- $\boldsymbol{y}_P$: joint design vector for joints between plate components

- $\boldsymbol{y}_{BP}$: joint design vector for joints between beam and plate components

Decomposition vector for G_B, $\boldsymbol{x}_B$ represents the *non*-existence of a joint (*i.e.*, the existence of a solid connection) at each connection of two basic members (an edge in the structural topology graph) in a structure represented by G_B:

$$\boldsymbol{x}_B = (x_{B\,0}, x_{B\,1}, \ldots, x_{B\,i}, \ldots, x_{B\,nB-1}) \tag{1}$$

where $nB = |E_\mathrm{B}|$ and

$$x_{B\,i} = \begin{cases} 0 & \text{if edge } e_{Bi} \text{ is removed in } G_B \\ 1 & \text{otherwise} \end{cases} \tag{2}$$

Decomposition vector for G_P, $\boldsymbol{x}_P$ is similarly defined, by replacing the subscript B with P.

Joint design vectors $\boldsymbol{y}_B$ represents the joint designs between beam two components:

$$\boldsymbol{y}_B = (\boldsymbol{y}_{B\,0}, \boldsymbol{y}_{B\,1}, \ldots, \boldsymbol{y}_{B\,i}, \ldots, \boldsymbol{y}_{B\,nB-1}) \tag{3}$$

Elements of vector $\boldsymbol{y}_B$ are in turn defined as vector $\boldsymbol{y}_{B\,i} = (y_{Bi\,0}, y_{Bi\,1}, \ldots, y_{Bi\,j}, \ldots, y_{Bi\,\mathrm{n-1}}) \in \boldsymbol{F}_B$, which represents $\mathrm{J}_{\mathrm{eB}i}$ (joint design corresponding to i^{th} edge $\mathrm{e}_{\mathrm{B}i}$ in G_B) from the feasible beam joint design set $\boldsymbol{F}_B$. Since joints are modeled as torsional springs, joint design $\boldsymbol{y}_{Bi}$ represents a vector of the torsional springs rates [Nm/rad]. For 3D, a joint requires three design variables (rotations around spring x, y, and z axes) and $\boldsymbol{y}_{B\,i} = (y_{Bi\,0}, y_{Bi\,1}, y_{Bi\,2}) = (k_{\mathrm{i}\,x}, k_{\mathrm{i}\,y}, k_{\mathrm{i}\,z})$. However, joint attribute $\boldsymbol{y}_{Bi}$ is considered only when i^{th} edge $\mathrm{e}_{\mathrm{B}i}$ is removed in G_B. Joint design vector $\boldsymbol{y}_P$ for plate components is similarly defined, by replacing the subscript B with P.

Element of vector $\boldsymbol{y}_{BP}$ is also defined similarly, by replacing subscript B with BP. However, unlike to the previous $\boldsymbol{y}_{B\,i}$ and $\boldsymbol{y}_{B\,i}$, every joint attribute $\mathrm{J}_{\mathrm{eBP}i}$ is considered and realized in the FE model. The reason is because it is assumed that there always exist a joint between beam component and plate components (in other words, beam and plate can not form one component together).

Definition of objective functions

A multi-component structure represented by two decomposition vector $\boldsymbol{x}_B$ and $\boldsymbol{x}_P$ and three joint design vectors $\boldsymbol{y}_B$, $\boldsymbol{y}_P$, and $\boldsymbol{y}_{BP}$ is evaluated according to the following three objectives: 1) stiffness of the assembled structure under given loading conditions, 2) manufacturability of components, and 3) assembleability of components.

The first objective function, $f_{\mathrm{stiffness}}$, evaluates stiffness (to be maximized) of the assembled structure. Stiffness of the structure can be measured as the negative of the displacement at predefined points in the structure:

$$f_{\mathrm{stiffness}} = -\mathrm{DISPLACEMENTS}(G_B(\boldsymbol{x}_B), G_P(\boldsymbol{x}_P), \boldsymbol{y}_B, \boldsymbol{y}_P, \boldsymbol{y}_{BP}) \tag{4}$$

where DISPLACEMENTS is a function that returns the total displacements at predefined points of in FE model defined by the decomposed $G_B(\boldsymbol{x}_B)$, $G_P(\boldsymbol{x}_P)$, and three joint design vectors $\boldsymbol{y}_B$, $\boldsymbol{y}_P$, and $\boldsymbol{y}_{BP}$.

The second objective function, f_{manufac}, evaluates manufacturability (to be maximized) of the set of components considering the total cost of producing components in the structure represented by the decomposed $G_B(\boldsymbol{x}_B)$ and $G_P(\boldsymbol{x}_P)$. As stated before, components are assumed to be made from sheet metals working, whose cost is estimated as the cost of stamping and blanking dies. Following equation is used to calculate manufacturability of a structure:

$$f_{\mathrm{manufac}} = -\Big\{ \sum_{i=1}^{nBC} \mathrm{DIECOST_B}(\mathrm{Au}(\mathrm{COMP_B}(i, G_B(\boldsymbol{x}_B)))) + \sum_{j=1}^{nPC} \mathrm{DIECOST_P}(\mathrm{Au}(\mathrm{COMP_P}(j, G_P(\boldsymbol{x}_P)))) \Big\} \tag{5}$$

where $\mathrm{COMP_B}(i, G_B(\boldsymbol{x}_B))$ and $\mathrm{COMP_P}(j, G_P(\boldsymbol{x}_P))$ return the i^{th} component of beam structure defined by the decomposed $G_B(\boldsymbol{x}_B)$ and the j^{th} component of plate structure defined by the decomposed $G_P(\boldsymbol{x}_P)$, respectively. Au(C) is a function returns the die useable area of a component C. $\mathrm{DIECOST_B}(A)$ and $\mathrm{DIECOST_P}(A)$ are the function calculates the die cost with given die useable area A for beam component and plated component, respectively. Finally, nBC and nPC are the numbers of the beam and plate components in the decomposed beam and plate substructures, respectively. Hence, f_{manufac} is considered as the negative sum of die cost for all components defined by two decomposition vector $\boldsymbol{x}_B$ and $\boldsymbol{x}_P$.

The third objective function, f_{assemble}, calculates assembleability (to be maximized) of the components. In this paper, assembleability is evaluated considering cost of assembly procedure, which is assumed to be spot welding. Since the cost of spot welding for a structure is proportional to the number of weld spots in the structure, and the number of weld spots in a joint is approximately proportional to the torsional stiffness of the joint, the welding cost is estimated by the sum of the rates of torsional springs [Nm/rad] in the FE model of the structure:

$$f_{\mathrm{assemble}} = -\mathrm{SPRINGRATE}(G_B(\boldsymbol{x}_B), G_P(\boldsymbol{x}_P), \boldsymbol{y}_B, \boldsymbol{y}_P, \boldsymbol{y}_{BP}) \tag{6}$$

where SPRINGRATE is the sum of the spring rates in FE model defined by the decomposed $G_B(\boldsymbol{x}_B)$, $G_P(\boldsymbol{x}_P)$, and three joint design vectors $\boldsymbol{y}_B$, $\boldsymbol{y}_P$, and $\boldsymbol{y}_{BP}$.

Formulation of optimization problem

The design variables and the objective functions defined in the previous sections provide the following multi-objective optimization problem:

maximize: $\{f_{\mathrm{stiffness}}, f_{\mathrm{manufac}}, f_{\mathrm{assemble}}\}$
subject to:

$$x_B \in \{0,1\}^{|E_B|}, x_P \in \{0,1\}^{|E_P|}$$
$$y_B \in F_B^{|E_B|}, y_P \in F_P^{|E_P|},$$
$$y_{BP} \in F_{BP}^{|E_{BP}|}$$

Note that there is no explicit constraint in this problem.

Optimization Algorithm

Due to the complexity of the underlying graph partitioning problem [28] and the multi-objective formulation without predefined weight or bounds on the objective functions, the above optimization problem is solved using a modified Non-Dominated Sorting Genetic Algorithm II (NSGA-II) [26]. This algorithm uses the non-dominated sorting method for Pareto ranking procedure, which successfully applied in our previous study [29].

A chromosome $\boldsymbol{c}$ (an internal representation of design variables for GA) is simply a list of the five design variables:

$$\boldsymbol{c} = (\boldsymbol{x}_B, \boldsymbol{x}_P, \boldsymbol{y}_B, \boldsymbol{y}_P, \boldsymbol{y}_{BP}) \tag{7}$$

Since information in the decomposition vectors ($\boldsymbol{x}_B$ and $\boldsymbol{x}_P$) and joint design vectors ($\boldsymbol{y}_B$, $\boldsymbol{y}_P$, and $\boldsymbol{y}_{BP}$) are linked in a non-linear fashion, the conventional one point or multiple point crossover for linear chromosomes [25] does not effectively preserve high-quality partial solutions (building blocks). For this type of problem, graph-based crossover has been successfully applied for improved performance of GA [4,5,29], which is modified to fit the current problem as described below:

1. Find the joint points which represent the physical locations of joints in two parent structures P1 and P2 (Figure 6)
2. Create an arbitrary plane A that "cut" the set of joint points of P1 into S1 and S2, and the set of joint points of P2 into S3 and S4 (Figure 7 (a) and (b)).
3. Construct two child structures C1 and C2 by "swapping" S2 and S4 (Figure 7 (c) and (d)) based on the decomposition and joint design of the parents.

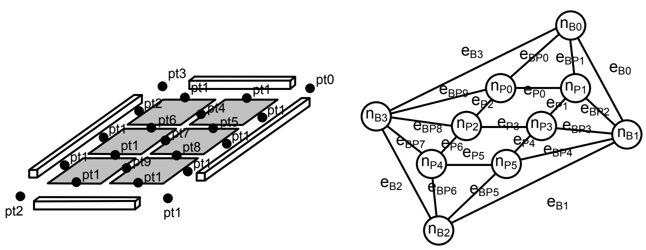

(a) (b)

edge	pt	edge	pt	edge	pt	edge	pt
e_{B0}	pt0	e_{P0}	pt4	e_{BP0}	pt11	e_{BP5}	pt16
e_{B1}	pt1	e_{P1}	pt5	e_{BP1}	pt12	e_{BP6}	pt17
e_{B2}	pt2	e_{P2}	pt6	e_{BP2}	pt13	e_{BP7}	pt18
e_{B3}	pt3	e_{P3}	pt7	e_{BP3}	pt14	e_{BP8}	pt19
		e_{P4}	pt8	e_{BP4}	pt15	e_{BP9}	pt20
		e_{P5}	pt9				
		e_{P6}	pt10				

(c)

Figure 6. (a) Physical location of joints. (b) Entire structural graph G_E. (c) Table of Joint points and corresponding edges in G_E.

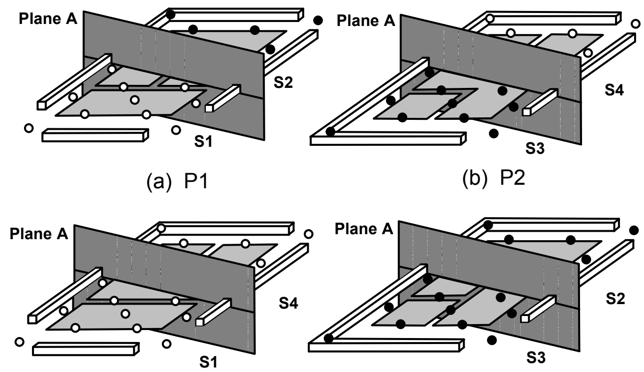

(a) P1 (b) P2

(c) C1 (d) C2

Figure 7. "Graph-based" crossover operation by plane A. (a) parent structures P1 cut into S1/S2, (b) another parent structure P2 cut into S3/S4, (c) child C1 made of S1/S4, and (d) child C2 made of S3/S2.

In addition to the above custom crossover, the implementation of NSGA-II used in this paper utilizes linear fitness scaling, niching based on the distances in objective function space, and stochastic universal sampling. Figure 8 shows the flowchart of the optimization. Software implementation, including NSGA-II code, is done in the C++ programming language. LEDA library was used for graph algorithm and commercial FEM software, MSC NASTRAN is used to obtain $f_{\text{stiffness}}$.

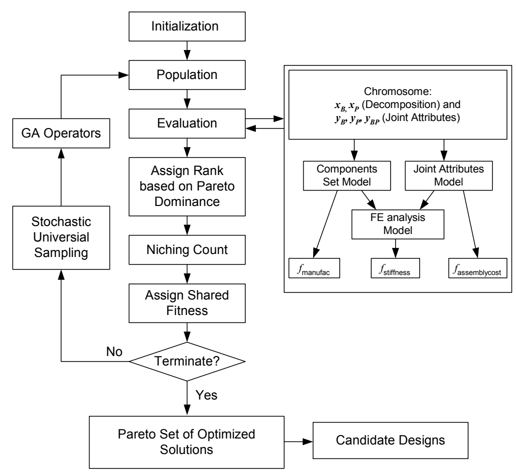

Figure 8. Flowchart of multi-component structure synthesis.

CASE STUDIES

Two case studies are discussed in this section. In the first case study, the side frame of a FE model of a 4 door passenger vehicle BIW (Figure 9 and Table 1) is decomposed for the minimum distortion of front door geometry under global bending. In the second case study, the side frame and floor panels of the same FE model are simultaneously decomposed for the minimum floor deflection under global bending. The FE model is composed of beam and plate elements. Table 2 lists the parameters values for GA used in the case studies.

These parameters were selected considering the convergence trend of the number of individuals in the Pareto Front.

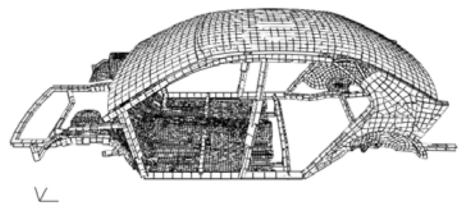

Figure 9. FE model of a 4 door passenger vehicle BIW composed of beam and plate elements.

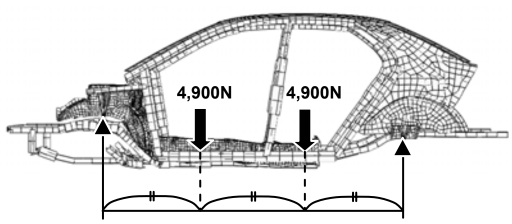

Figure 10. Global bending condition use for Case Studies I and II. Two downward loads of 4,900 [N] (1/4 of total weight) are applied at nodes on rocker at the 1/3 distance between supports.

Table 1. Properties of BIW model used in Case Studies I and II

Properties	*Count*
DOF	108,672
GRID	20,507
CBEAM	597
CQUAD4	15,788
CTRIA3	1,160

Table 2. Parameter values of GA in Case Studies I and II

Property	Value
maximum # of generation	100
number of population	300
replacement rate (m/n)	0.5
crossover probability	0.9
mutation probability	0.10

In both case studies, the following assumptions are made:

1. Body is subject to a global bending due to the weight of the vehicle (Figure 10).
2. Components are symmetric in the left and fight sides of the body.
3. Components are joined with spot welds modeled as three torsional springs whose axes of rotations are parallel to the 3 axes in global Cartesian coordinate system where x, y, and z directions are aligned along the length, width and height of the car model.

Case Study I: Side Frame

Figure 11 (a) shows the side frame portion of the BIW model to be decomposed, which consists of beam elements. Using the symmetry, 21 basic members (Figure 11 (b)) were selected from one side frame. Figure 11 (c) shows corresponding entire structural graph G_E with 21 nodes and 24 edges, which is identical G_B since there are only beam elements.

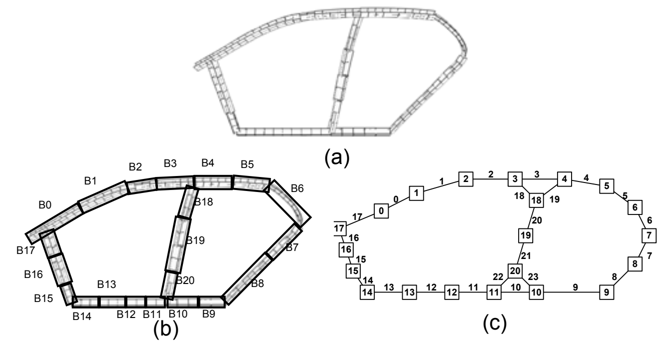

Figure 11. (a) side frame portion of the FE model made of beam elements, (b) selected 21 basic members, and (c) corresponding entire structural topology graph G_E with 21 nodes and 24 edges.

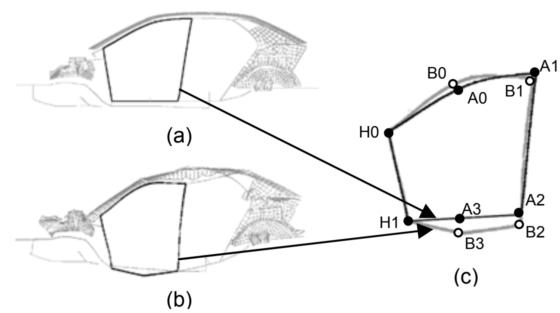

Figure 12. (a) side frame before deformation and (b) after deformation, and (c) calculation of front door frame distortion. Black line: front door shape in (a) and gray line: front door shape in (b). DISPLACEMENTS **will be the maximum distance between** A*i* **and** B*i* **(*i*=0,1,2,3).**

Under any loading conditions, the front door frame should retain its original shape with minimal distortion to guarantee the normal door opening and closing. In this case study, the stiffness function estimates the distortion of the deformed front door frame. Original (Figure 12 (a)) and deformed front door frame profile (Figure 12 (b)) are placed on each other for the hinge points (H0 and H1 in Figure 12 (c)) to keep minimum distances (Figure 12 (c)). Distortion of the deformed front door frame is calculated by measuring the distances between pre-specified points in the original front door frame profile and corresponding points in the deformed front door frame profile. Based on this consideration, DISPLACEMENTS function that determines $f_{\text{stiffness}}$ in Equation 6 is defined as:

$$\text{DISPLACEMENTS}(G_B(\boldsymbol{x}_B), G_P(\boldsymbol{x}_P), \boldsymbol{y}_B, \boldsymbol{y}_P, \boldsymbol{y}_{BP}) = \max_{i\in\{0,1,2,3\}} (\overline{AiBi}) \tag{8}$$

where A*i* and B*i* (*i*=0…3) are location of a point in the front door frame before and after deformation, respectively.

Figure 13 shows GUI of the developed software for Case Study I showing the Pareto solutions at the terminal generation (100). Because there are three objective functions $f_{\text{stiffness}}$, f_{manufac}, and f_{assemble}, the resulting 3-dimensional function space is projected on to three 2-dimensional spaces as shown in Figures 14 (a)-(c). Each 2-D plot shows points for all 300 structural designs with respect to the chosen two objectives only, ignoring the values of the remaining one objective. In all plots, the utopia points are located at the upper right corner. 4 representative designs (R1-R4) are selected from the Pareto front and each design is illustrated in the Figure 15-18. The following observations are made on these designs:

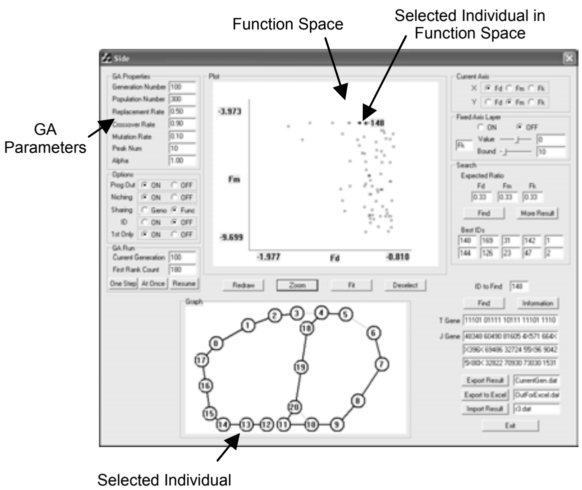

Figure 13. GUI of the optimization software used in Case Study I.

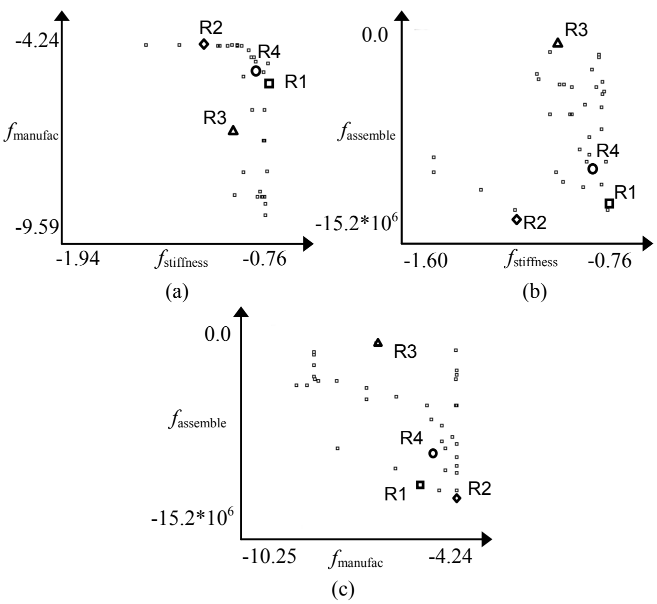

Figure 14. Function values at the terminal generation (generation number = 100). Points in the plots are the Pareto optimal designs.

- Design R1 (Figure 15) shows the best design considering only $f_{\mathrm{stiffness}}$ with 4 components that preserve the front door frame shape most close to the original front door frame shape by having no joints between the B-Pillar and the connecting positions of Roof Rail and Rocker Rail. Rear door frames includes 3 joints with small value of torsional spring rates allowing the rear door frame to absorb most distortion and leave the front door frame relatively undistorted.
- Design R2 (Figure 16) shows the best design considering only f_{manufac}. This 6 component design shows the best manufacturability by having all components in linear shape which minimizes the die usable area.
- Design R3 (Figure 17) shows the best design considering only f_{assemble}. It is composed of only one component, which eliminated the joint in the structure, resulting minimum cost of assembly. Note this design is not best for $f_{\mathrm{stiffness}}$, since this total rigid design without a compliant rear door frame causes more distortion in front door frame than R1.
- Design R4 (Figure 18) shows the design considering all three objectives. Similar to R1, this 5 components design preserves the front door frame shape relatively undistorted by having no joints between the B-Pillar and Roof Rail/Rocker Rail. Also, all 5 components are relatively in linear shape to minimize the die usable area, which decide the total cost of manufacturing. As Spider diagram in Figure 19 indicates, it is the most balanced design in all 3 objectives.

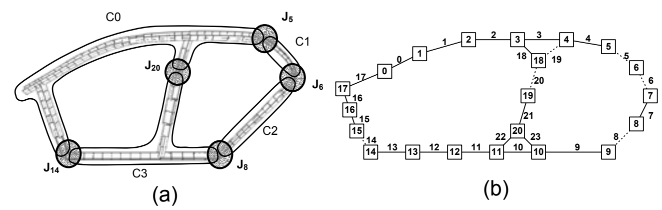

JD	k_x	k_y	k_z
J_5	0.8	0.001	0.3
J_6	1.0	0.001	0.3
J_8	0.5	0.2	0.2
J_{14}	0.5	0.6	0.6
J_{20}	0.7	0.001	0.7

*unit of k_x, k_y, k_z : [10^6 Nm/rad]

(c)

Figure 15. Design R1 (best $f_{\mathrm{stiffness}}$). (a) 4 components, (b) structural topology graph, and (c) joint designs.

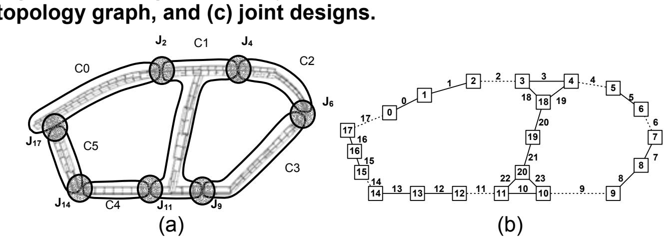

JD	k_x	k_y	k_z
J_2	0.3	0.001	0.9
J_4	0.4	0.2	0.1
J_6	0.1	0.5	0.1
J_9	0.2	0.001	0.4

JD	k_x	k_y	k_z
J_{11}	0.001	0.2	0.4
J_{14}	0.1	0.5	0.7
J_{17}	0.4	0.9	0.7

*unit of k_x, k_y, k_z : [10^6 Nm/rad]

(c)

Figure 16. Design R2 (best f_{manufac}). (a) 5 components (b) structural topology graph, and (c) joint designs.

Case Study II: Side/Floor Frame and Floor Panel

Figure 20 shows the side frames, floor frames and floor panel in the BIW model, composed of beam elements (CBEAM) and plate elements (CQUAD4 and CTRIA3). The half structure (Figure 21 (a) is divided into beam (Figure 21 (b)) and plate (Figure 21 (c)) substructures.

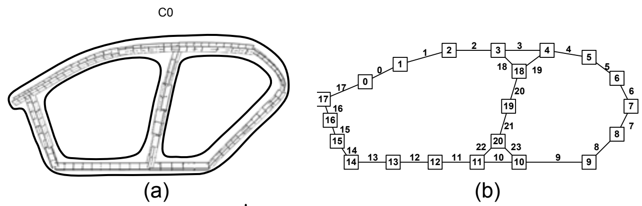

JD	k_x	k_y	k_z
N/A	N/A	N/A	N/A

*unit of k_x, k_y, k_z : [10^6 Nm/rad]

(c)

Figure 17. Design R3 (best f_{assemble}). (a) 1 component, (b) structural topology graph, and (c) joint designs: not available (no joints).

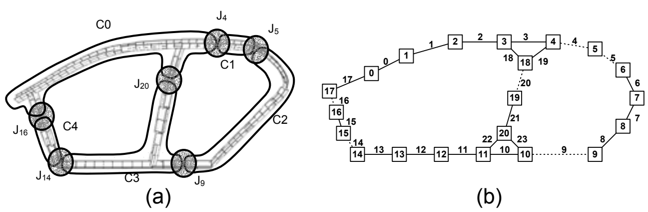

JD	k_x	k_y	k_z
J_4	0.2	0.7	0.7
J_5	0.1	0.2	0.1
J_9	0.3	0.001	0.5

JD	k_x	k_y	k_z
J_{14}	0.4	0.5	0.1
J_{16}	0.4	0.2	0.1
J_{20}	0.1	0.001	0.4

*unit of k_x, k_y, k_z : [10^6 Nm/rad]

(c)

Figure 18. Design R4. (a) 5 components (b) structural topology graph, and (c) joint designs.

Table 3. Objective function values for R1~R4.

	$f_{\text{stiffness}}$ [mm]	f_{manufac}	f_{assemble} [10*^{6}Nm/rad]
R1	-0.852	-5.573	-12.8
R2	-1.233	-4.477	-14.2
R3	-1.063	-6.878	0.0
R4	-0.919	-5.201	-10.0

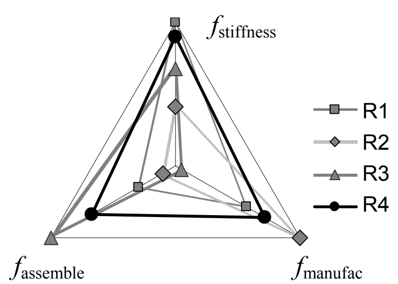

Figure 19. Spider Diagram of the 4 representative designs from the Pareto front in Case Study I, normalized within these 4 designs. Design R1, R2 and R3 show the best result only considering $f_{\text{stiffness}}$ value, f_{manufac} value, and f_{assemble} value, respectively. Design R4 shows balanced results in all 3 objective functions.

Total of 37 basic members and 28 basic members are defined on beam and plate substructures, as in Figure 22 and Figure 23, respectively, with corresponding structural topology graphs G_B and G_P. Graph G_B is made of 37 nodes and 46 edges and G_P is made of 28 nodes and 45 edges. Entire structural graph G_E is illustrated in Figure 24. It contains total 65 nodes and 120 edges, where 29 edges (edge 91 ~ edge 119) are used to connect between beam and plate basic members.

In this case study, the maximum downward deflection of the 4 points on the floor panel in Figure 25 is used in DISPLACEMENTS function:

$$\text{DISPLACEMENTS}(G_B(\boldsymbol{x}_B), G_P(\boldsymbol{x}_P), \boldsymbol{y}_B, \boldsymbol{y}_P, \boldsymbol{y}_{BP}) = \max_{i \in \{0,1,2,3\}} \textit{deflection}(Ai) \tag{9}$$

where *deflection*(Ai) is the downward deflection at point Ai.

Figure 26 illustrates GUI of the developed software and the objective function values obtained at the terminal generation (= 100) are illustrated in Figure 27. As in Case Study I, each 2-D plot shows the points in the 3D Pareto front with respect to the chosen two objectives only, ignoring the values of the remaining one objective. In all plots, the utopia points are located at the upper right corner.

Four representative designs (R1-R4) are selected from the Pareto front and each design isillustrated in Figures 28-31. The following observations are made on these designs:

- Design R1 (Figure 28) shows the best design considering only $f_{\text{stiffness}}$ with a big size floor frame component (CB2) and one piece panel component (CP1), which helped increase entire structural rigidity. However, by having one piece floor panel component sacrificed total manufacturability compared with the other 3 designs as shown in Figure 32.
- Design R2 (Figure 29) shows the best design considering only f_{manufac}. It contains 8 beam components whose shapes are relatively linear which minimizes the die usable area for each component. However, by having more number of joints in the beam structure, this design shows worst floor deflection compared with the other 3 designs.
- Design R3 (Figure 30) shows the best design considering only f_{assemble}. It contains one piece floor panel component which minimizes the use of joints in the floor panel and also minimizes the assembly cost. In the beam structure, it contains relatively small number of components (4) and joints (Figure 30 (e)-(g)) has smaller torsional spring rates. Smaller torsional spring rates indicate smaller number of spot welds, which also minimize the assembly cost. As in R1, by having one piece floor panel component, total manufacturability of structure was sacrificed compared with the other 3 designs.
- Design R4 (Figure 31) shows the design considering all three objectives. This design achieves relatively small floor panel deflection by component CB6 (Figure 31 (a)) containing one of loading points. Having the loading point isolated in a small component seems to localize the effect of loading, resulting small value of deflection. All 7 beam components are in linear shape, which minimized the manufacturability. Spider diagram in Figure 33 indicates that design R4 is balanced in all three objectives compared with the other 3 designs.

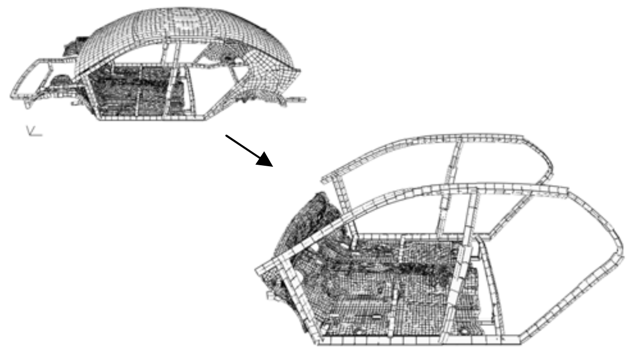

Figure 20. Side/floor frame and floor panel in BIW model used in Case Study II.

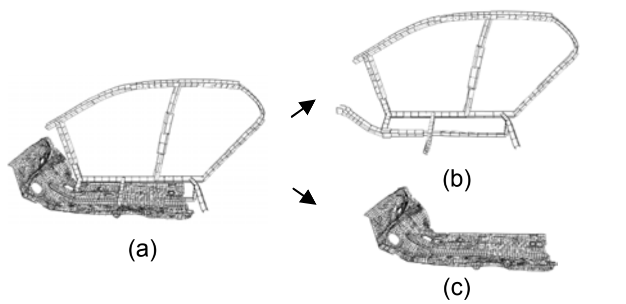

Figure 21. (a) Entire structure to be decomposed (right half only), (b) beam substructure, and (c) plate substructure.

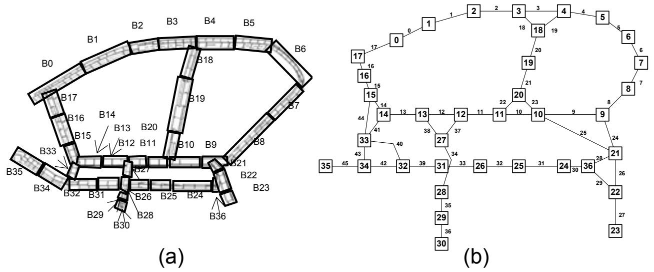

Figure 22. (a) 37 basic members in beam substructure and (b) corresponding structural topology graph G_B with 37 nodes and 46 edges.

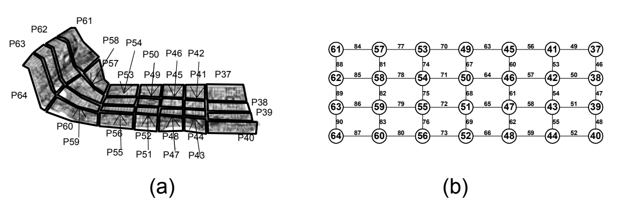

Figure 23. (a) 28 basic members in plate substructure and (b) corresponding structural topology graph G_P with 28 nodes and 45 edges.

SUMMARY AND FUTURE WORK

This paper described a method for synthesizing multi-component structural assemblies, where the three dimensional finite element model of a vehicle body-in-white (BIW) is optimally decomposed into a set of components considering the stiffness of the assembled structure under given loading conditions, as well as the manufacturability and assembleability of components. Multi-objective genetic algorithm combined with graph-based crossover and FEM analyses was used to obtain Pareto optimal solutions for the three objectives. Two case studies on 3D BIW model were presented to demonstrate the effectiveness of the proposed method.

ACKNOWLEDGMENTS

The authors acknowledge funding provided by Toyota Motor Corporation and National Science Foundation under CAREER Award (DMI-9984606) for this research. Any opinions, findings, and conclusions or recommendations expressed in this material are those of the authors and do not necessarily reflect the views of the National Science Foundation.

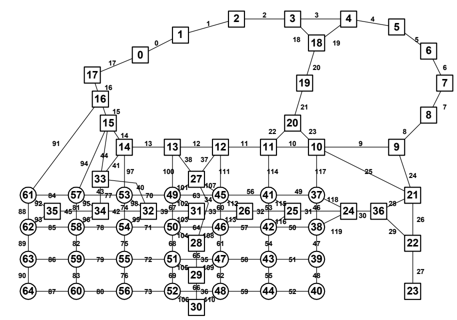

Figure 24. Entire structural graph G_E with 65 nodes and 120 edges. In G_E, 29 edges (edge 91~edge 119) are used to connect beam basic member and plate basic member.

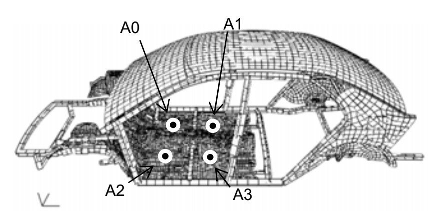

Figure 25. Points for measuring deflection of floor panel.

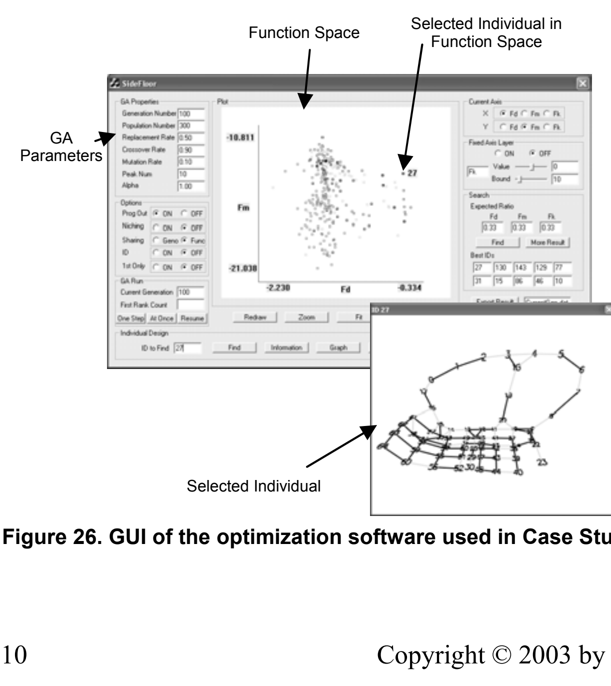

Figure 26. GUI of the optimization software used in Case Study II.

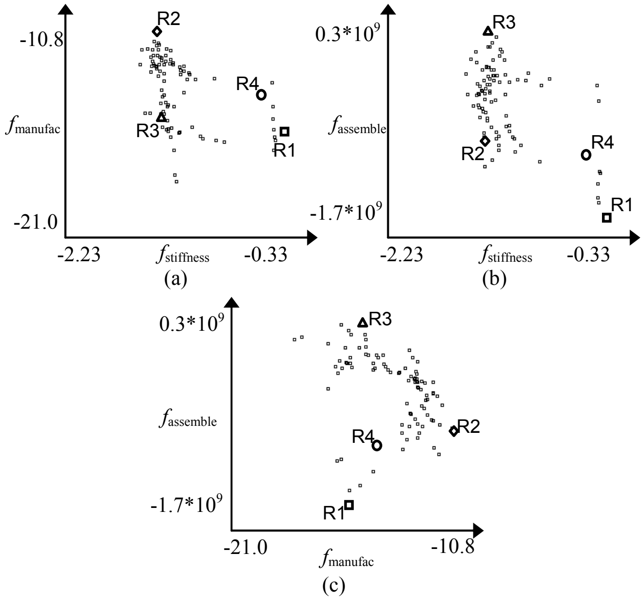

Figure 27. Function values at the terminal generation (generation number = 100). Points in the plots are the Pareto optimal designs.

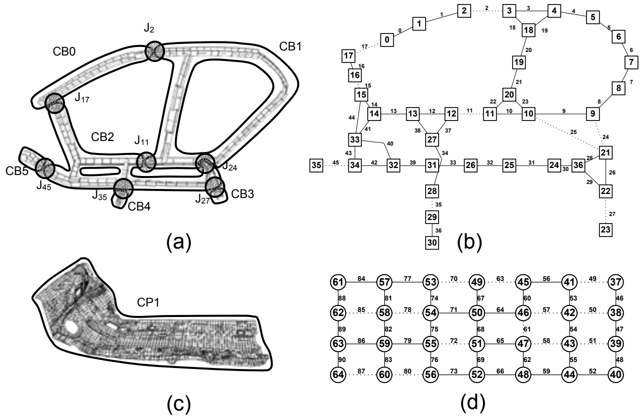

(e)

JD	k_x	k_y	k_z
J_{17}	0.2	0.6	0.3
J_{11}	1.0	1.0	0.9
J_{35}	1.0	0.8	0.6

(f)

JD	k_x	k_y	k_z
N/A	N/A	N/A	N/A

(g)

JD	k_x	k_y	k_z
J_{100}	0.7	0.5	0.6
J_{112}	1.0	0.9	0.9
J_{117}	0.8	0.8	0.9

*unit of k_x, k_y, k_z : [10^6 Nm/rad]

Figure 28. Design R1 (best $f_{\text{stiffness}}$) (a) 6 components in beam substructure, (b) G_B, (c) 1 component in plate substructure, (d) G_P. (e) joint designs (selected from 7 joints) in beam substructure, (f) joint designs in plate substructure: not available (no joints), and (g) joint designs (selected from 29 joints) between beam and plate substructures.

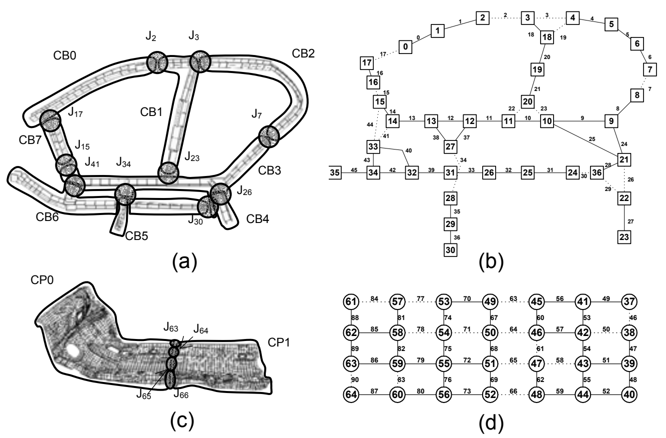

(e)

JD	k_x	k_y	k_z
J_2	0.5	1.0	0.1
J_{23}	0.1	0.7	0.8
J_{41}	0.8	0.7	0.4

(f)

JD	k_x	k_y	k_z
J_{63}	0.5	0.7	0.8
J_{64}	0.9	0.6	0.8
J_{65}	0.9	0.9	0.4

(g)

JD	k_x	k_y	k_z
J_{100}	0.2	0.7	0.1
J_{112}	0.1	0.9	0.1
J_{117}	0.3	0.1	0.3

*unit of k_x, k_y, k_z : [10^6 Nm/rad]

Figure 29. Design R2 (best f_{manufac}) (a) 8 components in beam substructure, (b) G_B. (c) 2 components in plate structure, (d) G_P. (e) 3 joint designs (selected from 10 joints) in beam substructure, (f) 3 joint designs (selected from 4 joints) in plate substructure, (g) 3 joint designs (selected from 29 joints) between beam and plate structures.

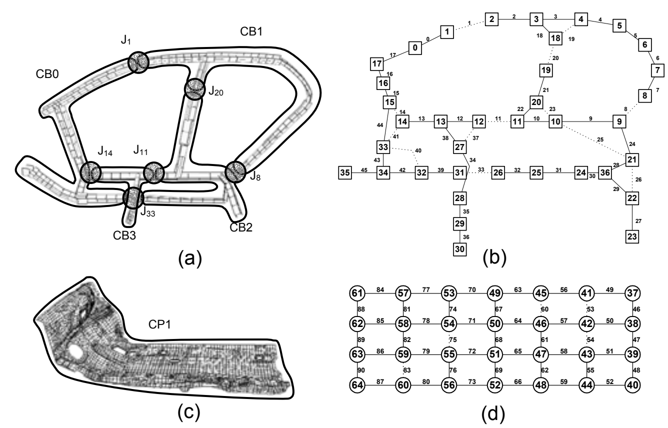

(e)

JD	k_x	k_y	k_z
J_1	0.6	0.3	0.2
J_{20}	0.3	0.2	0.4
J_{33}	0.5	0.4	0.001

(f)

JD	k_x	k_y	k_z
N/A	N/A	N/A	N/A

(g)

JD	k_x	k_y	k_z
J_{100}	0.001	0.3	0.2
J_{112}	0.5	0.2	0.2
J_{117}	0.3	0.001	0.001

*unit of k_x, k_y, k_z : [10^6 Nm/rad]

Figure 30. Design R3 (best f_{assemble}). (a) 4 components in beam substructure, (b) G_B., (c) 1 component in plate substructure, (d) G_P. (e) 3 joint designs (selected from 6 joints) in beam substructure, (f) joint designs in plate substructure: not available (no joints), (g) 3 joint designs (selected from 29 joints) between beam and plate structures.

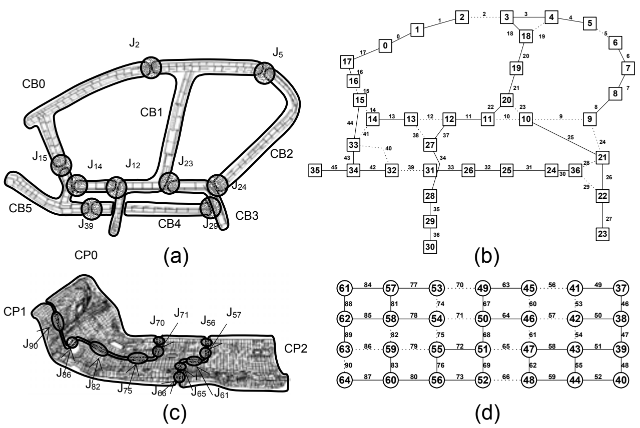

JD	k_x	k_y	k_z
J_{12}	0.1	0.9	0.001
J_{15}	0.001	0.5	0.3
J_{39}	0.001	0.3	0.4

(e)

JD	k_x	k_y	k_z
J_{57}	0.4	0.2	0.6
J_{71}	0.9	0.3	0.7
J_{90}	0.9	1.0	0.6

(f)

JD	k_x	k_y	k_z
J_{100}	0.1	0.4	0.001
J_{112}	0.2	1.0	0.3
J_{117}	0.2	0.3	0.3

(g)

*unit of k_x, k_y, k_z : [10^6 Nm/rad]

Figure 31. Design R4. (a) 7 components in beam substructure, (b) G_B, (c) 3 components in plate substructure, (d) G_P, (e) 3 joint designs (selected from 9 joints) in beam substructure, (f) 3 joint designs (selected from 11 joints) in plate substructure, and (g) 3 joint designs (selected from 29 joints) between beam and plate structures.

Table 4. Objective function values for R1~R4.

	$f_{\text{stiffness}}$ [mm]	f_{manufac}	f_{assemble} [10^9Nm/rad]
R1	-0.333	-16.311	-1.683
R2	-1.543	-10.811	-1.084
R3	-1.427	-16.671	-0.308
R4	-0.534	-14.711	-1.192

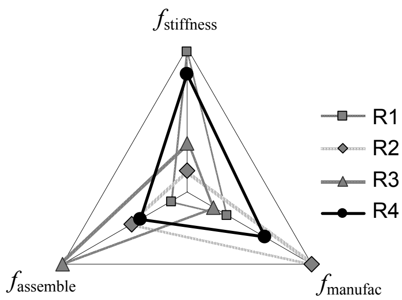

Figure 32. Spider Diagram of the 4 representative designs designs from the Pareto front in Case Study II, normalized within these 4 designs. Design R4 shows balanced results in all 3 objective functions.

REFERENCES

[1] Lyu, N. and Saitou, K., 2002. "Decomposition-based assembly synthesis based on structural stiffness considerations", *Proceedings of the 2002 ASME DETC*, September 29 - October 2, 2002, Montreal, Canada, DETC2002/DAC-34083. An extended version accepted to *ASME Journal of Mechanical Design.*

[2] Fonseca, C. M. and Fleming, P. J., 1993. "Genetic Algorithms for Multiobjective Optimization: Formulation, Discussion and Generalization", *Proceedings of the Fifth International Conference on Genetic Algorithms*, San Mateo, California, pp. 416-423.

[3] Coello , C. A., Veldhuizen, D. A. and Lamont, G. B., 2002. *Evolutionary algorithms for solving multi-objective problems,* Kluwer Academic/Plenum Publishers, New York. pp. 72.

[4] Laszewski, G., 1991. "Intelligent structural operators for the k-way graph partitioning problem", *Fourth International Conference on Genetic Algorithms*, pp. 45-52.

[5] Pereira, F., Machado, P., Costa, E., and Cardoso, A., 1999. "Graph Based Crossover – A Case Study with the Busy Beaver Problem", *Proceedings of the 1999 Genetic and Evolutionary Computation Conference*.

[6] Yetis, A. and Saitou, K., 2002. "Decomposition-Based Assembly Synthesis Based on Structural Considerations," *ASME Journal of Mechanical Design*, v. 124, pp. 593–601.

[7] Boothroyd, G. and Dewhurst, P., 1983. *Design for Assembly Handbook*, Univ. of Massachusetts, Amherst.

[8] Boothroyd, G., Dewhurst, P., and Knight, W., 1994. *Product Design for Manufacturing and Assembly*, Marcel Dekker, New York.

[9] Gupta, S. K., Regli, W. C., and Nau, D. S., 1994. "Integrating DFM with CAD through Design Critiquing", *Concurrent Engineering: Research and Application*, Vol. 2, pp.85-95.

[10] Ashley, S., "Steel cars face a weighty decision," *Mechanical Engineering*, Vol. 119(2), pp. 56-61, 1997.

[11] Barone, M. R, et al., 1981. *Modern Automotive Structural Analysis*; edited by Mounir M. Kamal and Joseph A. Wolf Jr., Van Nostrand Reinhold Co., New York.

[12] Kirioka, K., 1966. "An Analysis of Body Structures", *SAE Transactions*, Vol. 74, Paper No. 650026, pp.164-190.

[13] Brown, J. C., et al., 2002. *Motor Vehicle Structures: Concept and Fundamentals*, SAE International.

[14] Chang, D., 1974. "Effects of flexible connections on body structural response," *SAE Transactions*, Vol. 83, pp. 233-244.

[15] Garro, L. and Vullo, V., 1986. "Deformations car body joints under operating conditions", *SAE Transactions* 863197, pp. 5403-5420.

[16] Lee, K. and Nikolaidis, E., 1992. "A two-dimensional model for joints in vehicle structures", *Computers and Structures* 45 (4), pp.775-784.

[17] Lee, K. and Nikolaidis, E., 1998. "Effect of member length on the parameter estimates of joints," *Computers and Structures,* 68, pp. 381-391.

[18] Long, L., 1998. "Design-oriented Translators for Automotive Joints", PhD. Thesis, Virginia Polytechnic Institute.

[19] Kim, J., Kim, H., Kim, D., and Kim, Y., 2002. "New accurate efficient modeling techniques for the vibration analysis of T-joint thin-walled box structures", *International Journal of Solids and Structures*, Vol. 39, pp. 2893-2909.

[20] Coello , C. A., Veldhuizen, D. A. and Lamont, G. B., 2002. *Evolutionary algorithms for solving multi-objective problems*, Kluwer Academic/Plenum Publishers, New York.

[21] Fonseca, C. M. and Fleming, P.J., 1993. "Genetic Algorithms for Multiobjective Optimization: Formulation, Discussion and Generalization". In Forrest, S., editor, *Proceedings of the Fifth International Conference on Genetic Algorithms*, pp.416-423.

[22] Srinivas, N. and Deb, K., 1994. "Multiobjective Optimization Using Nondominated Sorting in Genetic Algorithms", *Evolutionary Computation*, 2(3), pp.221-248.

[23] Deb., K., Agrawal, S., Pratab, A., and Meyarivan, T.,2000. "A Fast Elitist Non-Dominated Sorting Genetic Algorithm for Multi-Objective Optimization: NSGA-II", KanGAL report 200001, Indian Institute of Technology, Kanpur, India.

[24] Horn, J., Nafpliotis, N., and Goldberg, D.E., 1994. "A Niched Pareto Genetic Algorithm for Multiobjective Optimization",

Proceedings of the First IEEE Conference on Evolutionary Computation, IEEE World Congress on Computational Intelligence, volume 1, pp.82-87.
[25] Goldberg, D. E., 1989. *Genetic Algorithms in Search, Optimization and Machine Learning*, Addison-Wesley Publishing Company, Massachusetts.
[26] Zitzler, E. and Thiele, L., 1998. “An Evolutionary Algorithm for Multiobjective Optimization: The Strength Pareto Approach”, *Technical Report* 43, Computer Engineering and Communication Networks Lab, Swiss Federal Institute of Technology, Zurich, Switzerland.
[27] Knowles, J.D. and Corne, D.W., 1999. “The Pareto Archived Evolution Strategy: A New Baseline Algorithm for Multiobjective Optimization”, In *1999 Congress on Evolutionary Computation*, pp.98-105, Washington, D.C.
[28] Garey, M. R. and Johnson, D. S., 1979. Computers And Intractability, a Guide to the Theory of NP-completeness, W. H. Freeman and Company, New York.
[29] Lyu, N. and Saitou, K., 2003. “Topology Optimization of Multi-component structures via Decomposition-based assembly synthesis”, *Proceedings of the 2003 ASME DETC*, September 2 - 6, 2003, Chicago, IL. DETC2003/DAC-48730.